High-speed light source depth estimation using spatially-resolved diffuse imaging

Kieran A. Brennan[1], **Daniel A.N. Kulasingham**[2], **Poul M.F. Nielsen**[1,2], **Andrew J. Taberner**[1,2], **and Bryan P. Ruddy**[1,2]

Auckland Bioengineering Institute, The University of Auckland, Auckland, NZ
Department of Engineering Science, The University of Auckland, Auckland, NZ

E-mail: kbre995@aucklanduni.ac.nz

September 2018

Abstract. We describe a system for high-speed depth estimation of a light source embedded in a scattering medium. A polynomial model estimates source depth from the spatially-resolved, diffuse reflectance profile measured with a fibre optic probe on the surface of a scattering medium. A dataset of Monte Carlo reflectance profiles is generated over a range of typical optical properties and the model is fit to the simulated reflectance at four detector locations. The model accounts for a source depth up to 15 mm. Cross-validation using the Monte Carlo dataset produced a root mean square error of 0.12 mm. Experimental reflectance data is acquired with the detector probe, which consists of four optical fibres mounted in a black acetal plastic disk. The optical fibres are coupled into avalanche photodiodes for high-speed acquisition of the reflectance profile. When applied to measurements from a tissue-mimicking phantom with an embedded light source, the polynomial model generates depth estimates within 2 mm of the true depth, up to a source depth of 15 mm.

Keywords: diffuse reflectance, turbid media, source location, tissue optics, Monte Carlo simulation.

1. Introduction

Diffuse optical techniques for characterising the properties and internal structure of biological tissue have been the subject of numerous research studies. Most notably, the method of diffuse optical tomography (DOT) has been used widely to identify absorbing or light-emitting features in a reconstructed, three-dimensional tissue volume [1, 2, 3]. DOT involves multiple diffuse light measurements with the sample illuminated from various locations. A simplification for local characterisation, spatially-resolved diffuse imaging (SRDI), involves tissue illuminated using a single light source. This technique has been widely applied to the problem of determining local optical properties, which can be used to recover the concentration of chromophores [4, 5, 6, 7]. Fewer studies have explored SRDI for recovering the location of light sources in tissue, with one group using

a fibre-based detector to make a spectrally dispersed measurement at 14 radial locations and a least-squares inversion of the diffusion model to estimate depth [8]. Two other groups have also successfully employed the diffusion model for depth estimation, on measurements obtained from a light source embedded in mice using specialised camera imaging systems [9, 10]. In this paper, we are particularly interested in estimating depth at high speed using a fibre-optic based measurement device. Such a system can be applied to large tissue volumes and is suitable for non-invasive monitoring of needle-free injection or robotic needle steering [11, 12, 13, 14]. This work describes a fibre-based probe for diffuse reflectance measurement, and an empirical inverse model for estimating source depth at high speed.

Fibre optic probes are widely used for diffuse reflectance measurements, particularly for local optical property estimation [15, 16, 17]. Probes typically consist of a single illumination fibre and several detector fibres with source-detector separations between 2 mm and 20 mm. While providing reduced spatial resolution when compared to camera-based systems, fibre-based probes are more suitable for larger samples as a portable system, which excludes ambient light when in contact with tissue. Typically, detector fibres are coupled into CCD detectors, point photodiodes, or spectrometers but such a device also offers the possibility of using highly sensitive point photodetectors such as avalanche photodiodes or vacuum photomultipliers [16, 18, 15].

Empirical inverse models, similar to what is proposed here, have been previously developed for the related problem of determining local optical properties. Farrell et al. trained a simple neural network to estimate optical properties from diffuse reflectance. Their neural network produced more robust estimates and solved 400 times faster than a gradient search fitting scheme based upon the diffusion model [19, 20]. A similar approach was taken more recently by Jäger et al., where multiple artificial neural networks, trained on Monte Carlo simulations, were able produce accurate optical property estimates with a computation time of less than a millisecond [21]. A different method, using a multiple polynomial regression model, has also been employed to estimate the optical properties of tissue using a fibre optic reflectance probe [16]. The model was calibrated directly on measurements from a series of control phantoms and was capable of estimating optical properties with errors less than 10 %. Furthermore, the optical property estimates could be computed in $\sim$ 50 ms and it was noted that a modern computer and compiled algorithm could significantly improve on this time. In the present study, a similar approach is taken where a polynomial function is fitted to Monte Carlo simulated data subsequently used for depth estimation rather than property estimation. The model is applied to reflectance measurements collected using a custom, high bandwidth fibre optic probe.

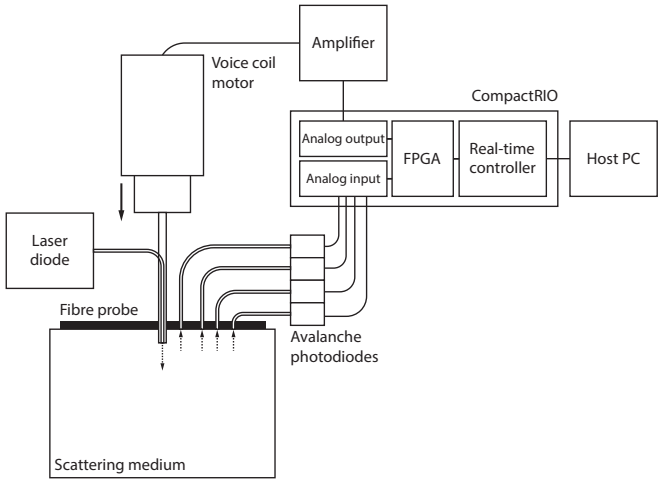

Figure 1. Depth-controlled light source experiments where a light emitting optical fibre is lowered into a tissue-mimicking phantom. The light source is guided through the centre of the fibre optic probe, which measures the resulting diffuse reflectance profile.

2. Materials and Methods

2.1. Fibre optic probe

The fibre optic probe consists of four silica-core optical fibres (200 μm core diameter, NA = 0.22) mounted into a black acetal disk (80 mm diameter) (figure 1). The acetal probe head provides a simple means of rigidly positioning the fibres, excludes ambient light, and imposes a controlled boundary condition. The fibres are coupled into four avalanche photodiode (APD) modules (Hamamatsu 2 $\times$ C12703-01, 2 $\times$ C5460-01). The detector fibres are fixed at distances of 3 mm, 5 mm, 7 mm, and 9 mm from the centre of the disk, while also being constrained to lie equidistant from the mounting point of an additional fibre, used to calibrate the photodetectors. Differences in manufacturing the probe and electrical characteristics of the photodetectors caused sensitivity differences between the detection channels. It was therefore necessary to determine the calibration factor for each detector pathway to normalise measurements to a common scale. This was achieved by placing the probe on a scattering medium and illuminating the medium through the calibration fibre. The radial symmetry of the resulting light distribution ensured each detector fibre was exposed to an equal intensity, and a calibration factor for each detector could be determined.

A depth-controlled light source was created with an optical fibre mounted to a position-controlled ($\pm$15 μm) voice-coil motor [22]. A flat-end, 20 gauge needle (0.9 mm outer diameter, 0.6 mm inner diameter) mounted to the motor provided a guide for the 200 μm optical fibre, which was positioned to protrude 0.5 mm from the end of the needle. The beam from an 808 nm laser diode was coupled into the fibre to provide a 5 mW, depth-controllable light source. A linear potentiometer was used to track the motor position ($\pm$15 μm) and a real-time controller (cRIO-9022, National Instruments)

controlled the trajectory of the source while simultaneously recording the output from the avalanche photodiodes at a sampling rate of 250 kHz.

The detector probe was positioned on the surface of a phantom (see below for formulation details) and the voice-coil motor was retracted to hold the source fibre at this location. The laser was energised, illuminating the scattering phantom through the source fibre, and a two-stage positioning procedure was performed: the source was held at the phantom surface for 20 ms while the surface-illuminated reflectance profile was acquired, followed by a 30 mm/s descent into the phantom to a maximum depth of 15 mm.

2.2. Diffusion model depth estimation

For comparison, depth-estimation results using the polynomial model, described below, were compared against a previously developed method using the diffusion model [23]. The details of the diffusion model depth estimation procedure are presented here briefly. The diffusion model has been solved for the geometry involving a point source in a semi-infinite, homogeneous medium (figure 2), where the radiance L (W/m^{2}sr) at the medium's surface is given by [4]:

$$L(\rho) = \frac{P}{16\pi^2 D}\Bigg(\frac{\exp(-\mu_{eff} r_1)}{r_1} - \frac{\exp(-\mu_{eff} r_2)}{r_2} + 3D\Big(\frac{d}{r_1^2}(\mu_{eff} + \frac{1}{r_1})\exp(-\mu_{eff} r_1) + \frac{d+2z_b}{r_2^2}(\mu_{eff} + \frac{1}{r_2})\exp(-\mu_{eff} r_2)\Big)\Bigg), \quad (1)$$

where ρ is the radial position on the medium surface, $D \equiv \frac{1}{3(\mu_s' + \mu_a)}$ is the diffusion coefficient, $\mu_{eff} \equiv \sqrt{3\mu_a(\mu_s' + \mu_a)}$, $\mu_s' \equiv (1-g)\mu_s$ is the reduced scattering coefficient, $z_b \equiv \frac{1+R_{eff}}{1-R_{eff}} 2D$, and R_{eff} is the effective reflection coefficient, which depends on the relative refractive index at the medium-air interface [4]. In the experimental configuration, the optical indices of the medium and measurement probe are assumed to be matched, meaning R_{eff} becomes zero.

To solve the inverse problem, a nonlinear least squares fitting procedure using the Levenberg-Marquardt algorithm was employed [23]. Three unknowns required estimation: the absorption coefficient, μ_a, the reduced scattering coefficient, μ_s', and the source depth, d, which were determined in two successive stages. Firstly, a characterisation step was performed, where the medium's optical properties were estimated with the light source incident on the top surface of the medium. Subsequently, with the source at an undetermined depth below the surface, the depth alone was found using the estimated optical properties.

The diffusion model depth estimation method was formulated to use the relative intensity profile to determine depth, meaning equation 1 was normalised when fitted to measured data. Under surface-illuminated conditions, the profile was normalised to the

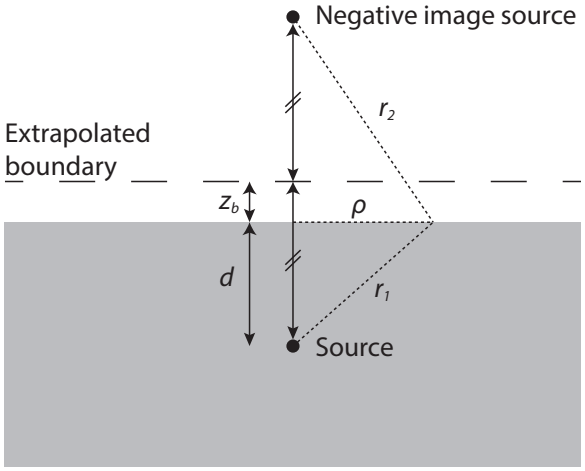

Figure 2. Solving the diffusion equation in a semi-infinite homogeneous medium using an extrapolated boundary condition.

value at the innermost radius, $L_{d=0}^{(\mathrm{exp})}(\rho_{norm})$, the nominal experimental normalisation factor. The function $L_{d=0}^{(\mathrm{mod})}(\rho)/L_{d=0}^{(\mathrm{mod})}(\rho_{norm})$ was then fitted to the data, thereby designating $L_{d=0}^{(\mathrm{mod})}(\rho_{norm})$ as the model normalisation factor. For all subsequent depth estimations, the reflectance profile was normalised by the experimental normalisation factor before the depth was determined using $L_d(\rho)/L_{d=0}^{(\mathrm{mod})}(\rho_{norm})$.

2.3. Polynomial model development

Monte Carlo simulations were used to generate a dataset of reflectance profiles to which the polynomial model could be fit. This provided a reference model of light propagation which enabled quick generation of a dense dataset while remaining straightforward to adapt to more complex geometries. A modified version of CUDAMCML, a GPU-based Monte Carlo routine [24, 25], was used to simulate a pencil beam light source at a prescribed depth in a single layer medium. The Henyey-Greenstein scattering phase function was used with an anisotropy parameter, g, of 0.9 for all runs [26, 27]. Simulations were performed with 17 absorption coefficients, μ_a, and 17 reduced scattering coefficients, μ_s', spanning the ranges: 0.01 mm^{-1} $\leq \mu_a \leq$ 0.15 mm^{-1} and 0.5 mm^{-1} $\leq \mu_s' \leq$ 2.0 mm^{-1}. A matched surface boundary condition was prescribed at the surface of the medium and 10^7 photons were used in each simulation. For each optical property set, simulations were performed with the source at depths from 0 mm to 15 mm in 0.5 mm increments. Thus, the dataset consisted of a total of 8959 simulations. The surface light intensity distribution output from the Monte Carlo simulation was convolved with a 0.2 mm, 2D top hat function using CONV [28] to match the size of the source fibre used in the experimental procedure, described below. The reflectance input values to the model were taken from radial positions of 3 mm, 5 mm, 7 mm, and 9 mm to match the measurement probe configuration. All reflectance data were $\log_{10}$ transformed before being input to the model.

Table 1. Optical Properties of the Scattering Phantoms

Trial	μ_a (mm^{-1})	μ_s' (mm^{-1})	c_{ink}(% v/v)	c_{int}(% v/v)
a	0.045	0.875	0.015	4.56
b	0.045	1.625	0.015	8.47
c	0.115	0.875	0.038	4.56
d	0.115	1.625	0.038	8.47

In order to accurately estimate source depth, the variability of the local optical properties must first be taken into account. The diffusion model depth estimation procedure, described above, involved an initial estimate of the absorption and scattering coefficients. However, for an empirical model, an explicit estimate of the optical properties is not strictly necessary. Instead, the confounding effect of local optical property variability can be isolated using the surface-illuminated reflectance profile as a direct input to the model. Thus, the polynomial model estimates depth in a single step with two sets of inputs: the surface-illuminated reflectance profile and the profile measured at the depth to be determined. A 3$^{\text{rd}}$-order polynomial was found to accurately recover source depth from the eight independent variables across the parameter space. With 8 independent variables, the polynomial model was formulated as:

$$P(x_i, x_j, ...x_p) = \sum_{i+j+...+p\leq 3} a_{ijk...p} x_1^i x_2^j \dots x_8^p, \tag{2}$$

involving 165 coefficients (one 0$^{\text{th}}$-order, eight 1$^{\text{st}}$-order, 36 2$^{\text{nd}}$-order, and 120 3$^{r\text{d}}$-order), which were determined using a least-squares fit to the Monte Carlo reflectance data with the source depth as the dependent variable. Subsequent depth estimation required only a straightforward function evaluation of equation 2 using the fitted coefficients.

In contrast to the diffusion model, the polynomial model used absolute reflectance profiles, which require the input to be in the same units as the Monte Carlo simulations (W/m^{2}sr). It was therefore necessary to scale the avalanche photodiode output to the units of the Monte Carlo simulation. The scale factor was determined by measuring the reflectance profile on a phantom with controlled optical properties and simulating the same conditions in a Monte Carlo simulation. The scale factor was then found by minimising the error between the two equivalent profiles in a least squares sense. All experimental data were subsequently scaled to the units of the Monte Carlo simulation before applying the polynomial model.

2.4. Tissue-mimicking Phantoms

Aqueous solutions of 20 % Intralipid (Fresenius Kabi) and Black India Ink (Higgins) were used as tissue-mimicking phantoms. A standardised procedure was used to create the phantoms, using linear interpolation to find the specific optical properties for 808 nm from the reference values [29]. Table 1 gives the nominal optical properties for the four experimental trials and the concentrations of India Ink, c_{ink} and Intralipid 20%, c_{int}.

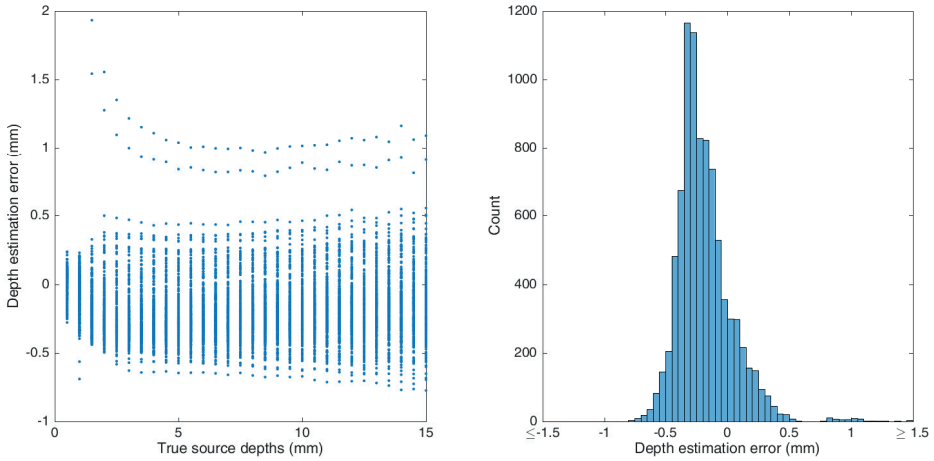

Figure 3. Depth estimation errors using the two-step diffusion model procedure. Left: Errors plotted against the true source depth. Right: Histogram showing the distribution of the depth errors. Errors beyond the range shown are accounted for in the edge bins.

3. Results

3.1. Cross validation

The two models were validated on the Monte Carlo dataset, described in Section 2.3, providing 8959 estimates to compare the accuracy of the models. The diffusion model estimation procedure was applied directly to the dataset, whereas for the polynomial model, leave-one-out cross-validation (LOOCV) was used to separate the test cases from the fitting dataset. This involved successively removing each data point from the set, fitting the model to the remaining data, and using the excluded point as a test case.

The diffusion model depth estimation model produces an RMS error of the estimates of 0.22 mm and with consistently small errors, remaining almost entirely within ± 1 mm (figure 3).

When performed using the polynomial model, LOOCV produced depth estimates that improved on the results from the method using the diffusion model (figure 4). For the full parameter space, the depth estimate rarely deviates more than 1 mm from the true depth value, with 99.4 % of the estimation errors within 0.5 mm. Furthermore, an RMS error of 0.12 mm demonstrates distinct improvement on the depth estimates using the diffusion model.

3.2. Experimental Results

When applied to the experimental data, the depth estimates using the diffusion model successfully track the true probe depth well for all four trials, remaining within 1 mm of the true depth up to a depth of 12 mm (figure 5). The 'step' consistently appearing in the depth estimate during the initial stages of the trajectory can be explained by examining

the least-squares objective function. Initially, a single minimum exists around a depth of zero that, as the source progresses into the medium, separates into two minima, with one tracking the progressively descending source. Until there is a distinct bifurcation, the minimum remains near zero and consequently the source depth is underestimated.

The two trials with the higher absorption coefficient (Trials c and d) produced noisy depth estimates as the probe depth approached 15 mm, appearing to approach the practical depth detection limit of the system at the given source power. As the signal-to-noise ratio depends on the attenuation of back-scattered light, the upper depth limit of this technique will depend on the optical properties of the medium, with the greatest depth range achieved when absorption is lowest and scattering is highest.

Depth estimates using the polynomial model produced estimates that remained within 2 mm of the actual depth for the entirety of each trajectory (figure 6). As a source depth of 15 mm is approached in Trial 4, the model produces a noisy estimate, likely due to the poor signal-to-noise ratio at these depths. The deviation of the depth estimate from the true source depth may arise due to discrepancies between the Monte Carlo and experimental settings, the major difference being the presence of an opaque needle to guide the light source in the phantom. There is also an additional source of error with the polynomial model in calculating the scaling factor between the experimental and Monte Carlo data, which may account for the increased error with the polynomial model. Regardless, the ability of the measurement system and polynomial model to track the source depth across four different media shows significant potential for a real-time depth estimation system, particularly given the simplicity of the model.

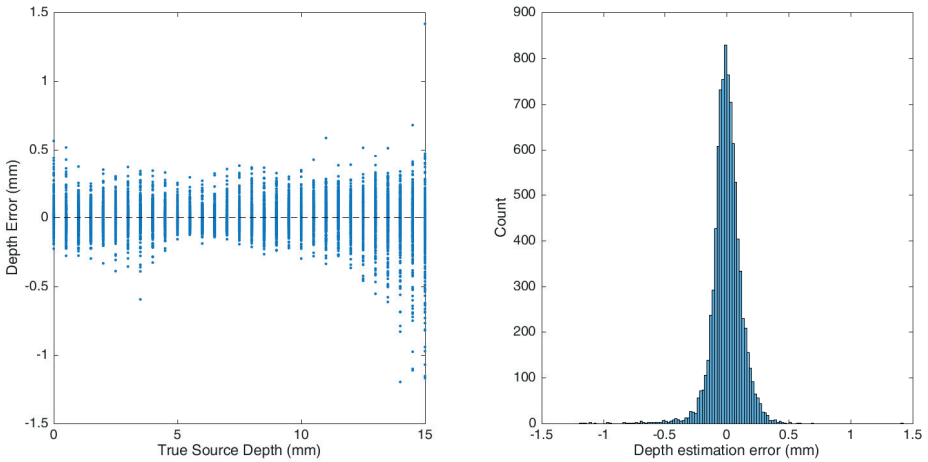

Figure 4. Depth estimation errors from LOOCV using the polynomial depth estimation model. Left: Depth errors plotted against the true source depth. Right: A histogram showing the depth error distribution.

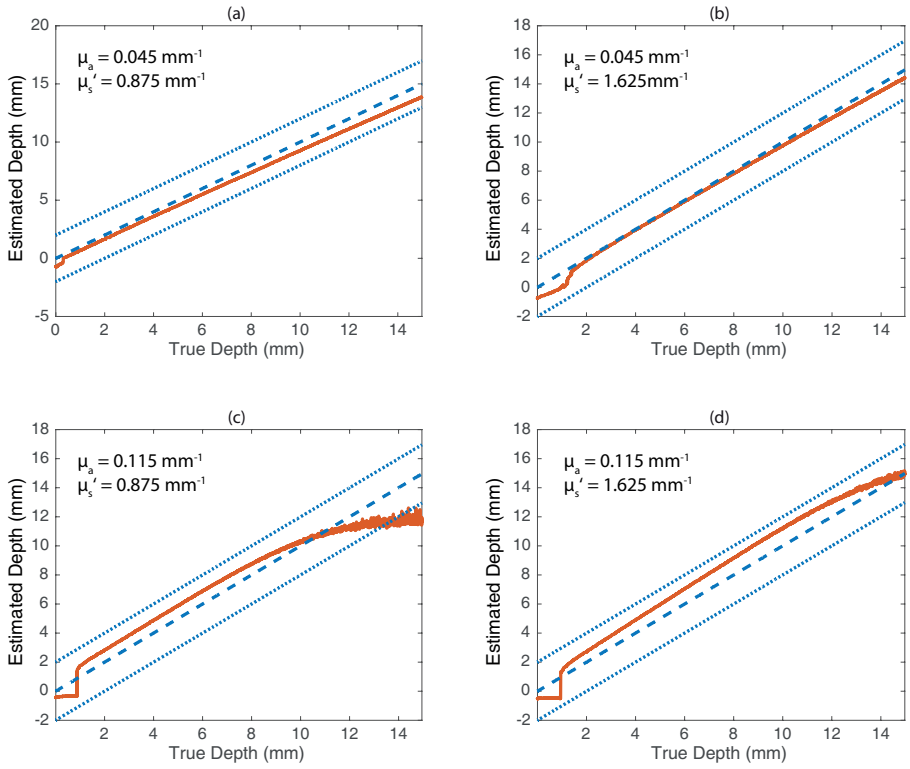

Figure 5. Diffusion model depth estimation from experimental reflectance profiles obtained from tissue-mimicking phantoms. The optical properties for trials a–d are listed in Table 1. The estimated source depth is shown as the solid line, the true probe depth is represented by the dashed line, and dotted lines border the ±2 mm error region.

4. Discussion and Conclusion

We have outlined a device for source depth estimation in a scattering medium using a high bandwidth, fibre-based probe to measure the reflectance profile and an empirical model for depth estimation. The model was fitted to a set of reflectance data, generated using Monte Carlo simulations, requires intensity data from four radial positions (3 mm, 5 mm, 7 mm, and 9 mm), and demonstrates superior accuracy to a diffusion model depth estimation procedure. Cross validation of the polynomial model using the Monte Carlo dataset produced an RMS error of 0.12 mm, with estimation errors typically less than 0.5 mm. When applied to experimental data, the depth estimation tracked the true source depth to within 2 mm, up to 15 mm into four phantoms with different optical properties. In the application of jet injection depth monitoring or robotic needle steering, this estimation accuracy could provide the means to control an intervention into the subcutaneous fat layer, which typically resides from as shallow as 2 mm to greater than 15 mm from the skin surface. Furthermore, the sensitive photodetectors permit high-speed sampling of the light distribution, requiring only a 0.1 ms averaging

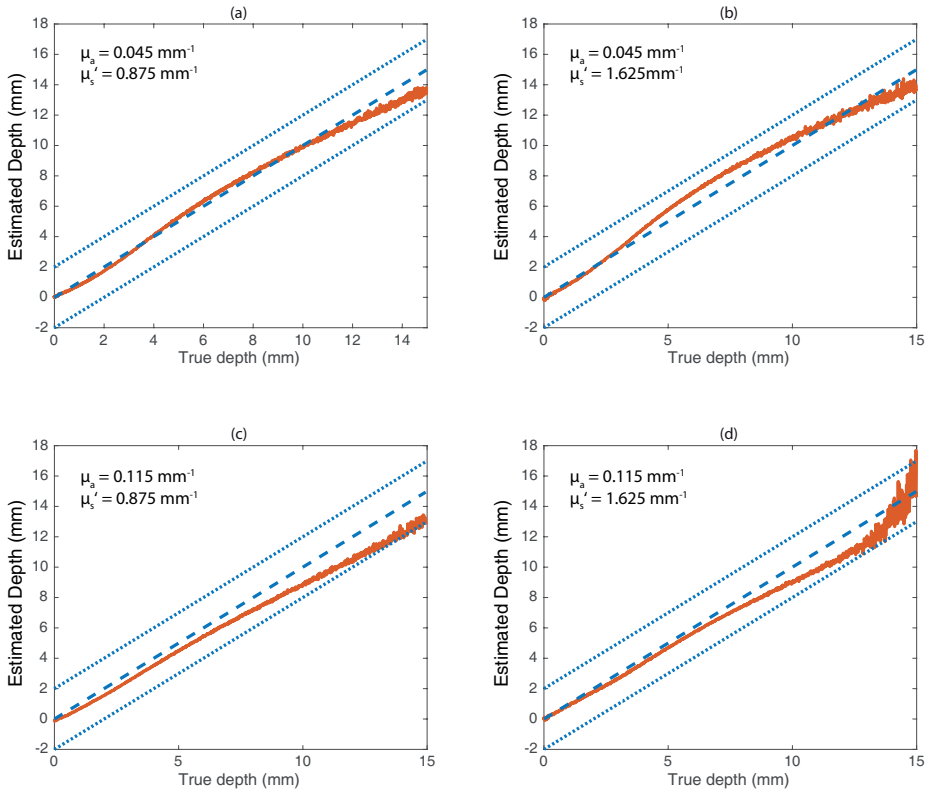

Figure 6. Polynomial model depth estimation from experimental reflectance profiles obtained from tissue-mimicking phantoms. The optical properties for trials a–d are listed in Table 1. The solid line shows the estimate, the dashed line shows the true source trajectory and dotted lines border the ±2 mm error region.

window. Thus, this method provides an estimation rate sufficient for jet injection depth monitoring or to inform a needle steering controller.

The polynomial model offers several advantages over the diffusion model. The diffusion model assumes that scattering outweighs absorption, while the Monte Carlo method does not rely on this premise. This may partly explain the poor performance of the diffusion model for Trial c (figure 5), where the absorption coefficient is highest and the scattering coefficient is lowest. In addition, the evaluation of the polynomial model is an inexpensive computation and could easily be implemented, for example, in an FPGA for real-time depth estimation. In contrast, depth estimation using the diffusion model requires a nonlinear fitting procedure, which typically requires 10 to 20 iterations of the Levenberg-Marquardt algorithm. Furthermore, the polynomial model offers the possibility to extend the complexity of the forward model. This is important as the models here have so far assumed the medium of interest possesses homogeneous optical properties, an unrealistic premise for biological tissue. Indeed, the optical properties of the layers comprising skin tissue — epidermis, dermis, and subcutaneous fat — can vary markedly across and between subjects [26]. Accurately characterising tissue properties

then tends towards an ill-posed problem as the number of free parameters in an N-layer medium becomes $3N-1$ when solving for μ_a, μ_s' and layer thickness (assuming a semi-infinite bottommost layer) [30]. However, the present scenario requires the estimation of only a single parameter and there remains the possibility that the presence of layered tissue does not heavily influence the ability to determine depth, as suggested by work simplifying the multilayer problem [31, 32, 18, 33]. Extending the geometry of the Monte Carlo forward model and performing simulations over the relevant parameter space will reveal the accuracy of this technique in multi-layer tissue, without necessarily increasing the complexity of the inverse model.

References

[1] David A. Boas, Dana H. Brooks, Eric L. Miller, Charles A. Dimarzio, Misha Kilmer, Richard J. Gaudette, and Quan Zhang. Imaging the body with diffuse optical tomography. *IEEE Signal Processing Magazine*, 18(6):57–75, 2001.

[2] Xiaoping Liang and Huabei Jiang. Experimental studies of near-infrared diffuse optical tomography in turbid media: Distributed excitation source and periodical boundary conditions coefficient. *Journal of Optics A: Pure and Applied Optics*, 6(4):454–460, 2004.

[3] Yong Xu, Qizhi Zhang, and Huabei Jiang. Optical image reconstruction of non-scattering and low scattering heterogeneities in turbid media based on the diffusion approximation model. *Journal of Optics A: Pure and Applied Optics*, 6(1):29–35, 2004.

[4] TJ Farrell, Michael S Patterson, and B C Wilson. A diffusion theory model of spatially resolved, steady-state diffuse reflectance for the noninvasive determination of tissue optical properties in vivo. *Medical physics*, 19(4):879–888, 1992.

[5] R M P Doornbos, R Lang, M C Aalders, F W Cross, and H J C M Sterenborg. The determination of in vivo human tissue optical properties and absolute chromophore concentrations using spatially resolved steady-state diffuse reflectance spectroscopy. *Physics in Medicine and Biology*, 44(4):967–981, 1999.

[6] Alexander Kokhanovsky and Ian Hopkinson. Some analytical approximations to radiative transfer theory and their application for the analysis of reflectance data. *Journal of Optics A: Pure and Applied Optics*, 10(3), 2008.

[7] William E Vargas. Inversion methods from Kubelka Munk. 452:4–9, 2002.

[8] E L Hull, M G Nichols, and T H Foster. Localization of Luminescent Inhomogeneities in Turbid Media with Spatially Resolved Measurements of CW Diffuse Luminescence Emittance. *Applied optics*, 37(13):2755–65, 1998.

[9] D. C. Comsa, T. J. Farrell, and M. S. Patterson. Quantification of bioluminescence images of point source objects using diffusion theory models. *Physics in Medicine and Biology*, 51(15):3733–3746, 2006.

[10] Olivier Coquoz, Tamara L Troy, Dragana Jekic-McMullen, and Bradley W Rice. Determination of depth of in vivo bioluminescent signals using spectral imaging techniques. In *Biomedical Optics*, pages 37–45. International Society for Optics and Photonics, 2003.

[11] Daniel Glozman and Moshe Shoham. Image-guided robotic flexible needle steering. *IEEE Transactions on Robotics*, 23(3):459–467, 2007.

[12] Zipi Neubach and Moshe Shoham. Ultrasound-guided robot for flexible needle steering. *IEEE Transactions on Biomedical Engineering*, 57(4):799–805, 2010.

[13] Andrew J. Taberner, Nathan B. Ball, N. Catherine Hogan, and Ian W. Hunter. A portable needle-free jet injector based on a custom high power-density voice-coil actuator. *Annual International Conference of the IEEE Engineering in Medicine and Biology - Proceedings*, pages 5001–5004, 2006.

[14] Andrew Taberner, N. Catherine Hogan, and Ian W. Hunter. Needle-free jet injection using real-time controlled linear Lorentz-force actuators. *Medical Engineering and Physics*, 34(9):1228–1235, 2012.

[15] Urs Utzinger and Rebecca R Richards-Kortum. Fiber optic probes for biomedical optical spectroscopy. *Journal of biomedical optics*, 8(1):121–47, 2003.

[16] J S Dam, C B Pedersen, T Dalgaard, P E Fabricius, P Aruna, and S Andersson-Engels. Fiber-optic probe for noninvasive real-time determination of tissue optical properties at multiple wavelengths. *Applied optics*, 40(7):1155–1164, 2001.

[17] Shao-Pow Lin, Lihong V Wang, Steven L Jacques, and Frank K. Tittel. Measurement of tissue optical properties by the use of oblique-incidence optical fiber reflectometry. *Applied Optics*, 36(1):136, 1997.

[18] Arianna Giusto, Cosimo D'andrea, Lorenzo Spinelli, Davide Contini, Alessandro Torricelli, Fabrizio Martelli, Giovanni Zaccanti, and Rinaldo Cubeddu. Monitoring absorption changes in a layered diffusive medium by white-light time-resolved reflectance spectroscopy. *IEEE Transactions on Instrumentation and Measurement*, 59(7):1925–1932, 2010.

[19] T J Farrell, B C Wilson, and M S Patterson. The use of a neural network to determine tissue optical properties from spatially resolved diffuse reflectance measurements. *Physics in Medicine and Biology*, 37(12):2281, 1992.

[20] Alwin Kienle, Lothar Lilge, Michael S Patterson, Raimund Hibst, Rudolf Steiner, and Brian C Wilson. Spatially resolved absolute diffuse reflectance measurements for noninvasive determination of the optical scattering and absorption coefficients of biological tissue. *Applied optics*, 35(13):2304–2314, 1996.

[21] Marion Jäger, Florian Foschum, and Alwin Kienle. Application of multiple artificial neural networks for the determination of the optical properties of turbid media. *Journal of Biomedical Optics*, 18(5):057005, 2013.

[22] Bryan P. Ruddy, Ian W. Hunter, and Andrew J. Taberner. Optimal Voice Coil Actuators for Needle-free Jet Injection. In *Engineering in Medicine and Biology Society (EMBC), 2014 36th Annual International Conference of the IEEE*, number 2, pages 2144–2148, 2014.

[23] Kieran A Brennan, Bryan P Ruddy, Poul M F Nielsen, and Andrew J Taberner. Light source depth estimation in porcine skin using spatially resolved diffuse imaging. In *2016 IEEE 38th Annual International Conference of the Engineering in Medicine and Biology Society (EMBC)*, pages 5917–5920, 2016.

[24] Lihong Wang, Steven L Jacquesa, and Liqiong Zhengb. MCML - Monte Carlo modeling of light transport in mutli-layered tissues. *Biomedicine*, 47(2):131–146, 1995.

[25] Erik Alerstam, Tomas Svensson, and Stefan Andersson-engels. Parallel computing with graphics processing units for high-speed Monte Carlo simulation of photon migration. 13(6), 2008.

[26] Valery Tuchin. *Tissue optics: light scattering methods and instruments for medical diagnosis*. SPIE Press, 3rd edition, 2015.

[27] S. K. Sharma and Srilekha Banerjee. Role of approximate phase functions in Monte Carlo simulation of light propagation in tissues. *Journal of Optics A: Pure and Applied Optics*, 5(3):294–302, 2003.

[28] Lihong Wang, Steven L. Jacques, and Liqiong Zheng. CONV - Convolution for responses to a finite diameter photon beam incident on multi-layered tissues. *Computer Methods and Programs in Biomedicine*, 54(3):141–150, 1997.

[29] Lorenzo Spinelli, M. Botwicz, N. Zolek, M. Kacprzak, D. Milej, Piotr Sawosz, Adam Liebert, U. Weigel, Turgut Durduran, Florian Foschum, Alwin Kienle, F. Baribeau, S. Leclair, J-P Bouchard, I. Noiseux, P. Gallant, Ozzy Mermut, Andrea Farina, Antonio Pifferi, Alessandro Torricelli, Rinaldo Cubeddu, H.-C. Ho, Mikhail Mazurenka, Heidrun Wabnitz, K. Klauenberg, O. Bodnar, C. Elster, M. Bénazech-Lavoué, Y. Bérubé-Lauzière, F. Lesage, D. Khoptyar, a. a. Subash, Stefan Andersson-Engels, Paola Di Ninni, Fabrizio Martelli, and Giovanni Zaccanti. Determination of reference values for optical properties of liquid phantoms based on Intralipid

and India ink. *Biomedical Optics Express*, 5(7):2037, 2014.

[30] Alwin Kienle, Michael S Patterson, Nora Dognitz, Roland Bays, Georges Wagnieres, and Hubert van den Berg. Noninvasive determination of the optical properties of two-layered turbid media. *Applied Optics*, 37(4):779–791, 1998.

[31] Setsuo Takatani and Marshall D. Graham. Theoretical analysis of diffuse reflectance from a two-layer tissue model. *IEEE transactions on bio-medical engineering*, 26(12):656–664, 1979.

[32] Dong Su Ho, Ee Hwa Kim, In Duk Hwang, Kunsoo Shin, Jung Taek Oh, and Beop Min Kim. Optical skin-fat thickness measurement using miniaturized chip LEDs: A preliminary human study. *Journal of the Optical Society of Korea*, 13(3):304–309, 2009.

[33] D. C. Comsa, T. J. Farrell, and M. S. Patterson. Bioluminescence imaging of point sources implanted in small animals post mortem: Evaluation of a method for estimating source strength and depth. *Physics in Medicine and Biology*, 52(17):5415–5428, 2007.